Analyst

ROYAL SOCIETY OF CHEMISTRY

PAPER

View Article Online
View Journal | View Issue

Cite this: *Analyst*, 2023, **148**, 1824

A highly effective "naked eye" colorimetric and fluorimetric curcumin-based fluorescent sensor for specific and sensitive detection of H_2O_2 *in vivo* and *in vitro*†

Wenhao Du, Zheyu Shen, Yueying Liang, Shuai Gong, Zhiyuan Meng, Mingxing Li, Zhonglong Wang* and Shifa Wang *

Hydrogen peroxide (H_2O_2) is involved in many important tasks in normal cell metabolism and signaling. However, abnormal levels of H_2O_2 are associated with the occurrence of several diseases. Therefore, it is important to develop a new method for the detection of H_2O_2 *in vivo* and *in vitro*. A turn-off sensor, 2,2-difluoro-4,6-bis(3-methoxy-4-((4-(4,4,5,5-tetramethyl-1,3,2-dioxaborolan-2-yl)benzyl)oxy)styryl)-2*H*-1,3,2-dioxaborine (**DFCB**), based on curcumin was developed for the detection of H_2O_2. The **DFCB**, an orange-emitting sensor, was constructed by employing 2,2-difluoro-4,6-bis(4-hydroxy-3-methoxystyryl)-2*H*-1,3,2-dioxaborine (**DFC**) as the main carrier, and 2-(4-bromomethylphenyl)-4,4,5,5-tetramethyl-1,3,2-doxaborolane as the recognition site. The recognition group on the **DFCB** sensor could be completely cleaved by H_2O_2 to generate the intermediate **DFC**, which would lead to a colorimetric change from bright orange to light blue accompanying by a significantly quenched fluorescence, which could be seen by the naked eye. This sensor exhibited a highly specific fluorescence response to H_2O_2, in preference to other relevant species, with an excellent anti-interference performance. The sensor **DFCB** also possessed some advantages including a wide pH response range (6–11), a broad linear range (0–300 μM), and a low detection limit (1.31 μM). The sensing mechanism of the **DFCB** sensor for H_2O_2 was verified by HRMS analysis, ^{1}H-NMR titration and DFT calculations. In addition, the use of the **DFCB** sensor was compatible with the fluorescence imaging of H_2O_2 in living cells and zebrafish.

Received 4th March 2023,
Accepted 9th March 2023

DOI: 10.1039/d3an00340j

rsc.li/analyst

Introduction

Hydrogen peroxide (H_2O_2) is one of the most important reactive oxygen species (ROS), and one of its key tasks is to activate immune cells and maintain the normal metabolism.[1–4] However, abnormal H_2O_2 generation will cause irreversible damage to the organism, and may attack cellular biomolecules such as protein and DNA,[5–10] affect cell metabolism and proliferation, and cause cancer, abnormal amino acid modification, Alzheimer's disease and other diseases.[11–13] Due to the complex pathologies that arise in organisms, H_2O_2 can cause oxidative stress and eventually lead to cell damage and necrosis.[14–16] Therefore, to develop efficient methods for detecting H_2O_2 is of great importance in disease prevention and medical diagnosis.

Existing quantitative detection methods, such as titrimetry, electrochemistry, spectrophotometry and so on, are relatively mature techniques.[17–19] Fluorescent sensor analysis has the advantages of fast response, strong selectivity, adaptability and microscopic properties, and it has been widely used for detecting some analytes in biological and environmental systems.[20–23] At present, there are many reported sensors for H_2O_2 which use aryl borate or phenyl boric acid reactions to generate phenol, phenol oxidation to give quinone, oxonium or diketone to give acid, carbon–carbon double bond breaking, and so on.[24–26] In recent years, a limited number of fluorescent sensors have been widely used for monitoring H_2O_2 in living organisms and cells.[27–30] However, some reported sensors for H_2O_2 have suffered from some drawbacks, such as unsatisfactory sensitivity, narrow pH usage range, and so on. Therefore, it is necessary to design pH-compatible fluorescent sensors for detecting H_2O_2 in biological systems.

Co-Innovation Center of Efficient Processing and Utilization of Forest Resources, International Innovation Center for Forest Chemicals and Materials, College of Chemical Engineering, Nanjing Forestry University, Nanjing, 210037, China. E-mail: wang_zhonglong@njfu.edu.cn, wangshifa65@163.com; Fax: +86-25-85428369; Tel: +86-25-85428369

† Electronic supplementary information (ESI) available. See DOI: https://doi.org/10.1039/d3an00340j

Curcumin, a natural product with a unique fluorescence nature, is found mainly in the rhizomes of the plant families Zingiberaceae and Araceae.[31,32] Curcumin has received much attention due to its wide range of health care functions and biological properties, such as antibacterial, anti-inflammatory, anti-infective, anti-cancer and liver protective activities. We propose that the curcumin-based fluorescent sensor may have low cytotoxicity.[33–35] Moreover, curcumin and its derivatives have a large conjugate structure, which could enhance the π electron delocalization. The curcumin and its derivatives are better to be emitted to generate outstanding long-wavelength fluorescence. The fluorescence sensor with a long-wavelength emission can effectively avoid interference with self-emission fluorescence, and is an ideal tool for *in vivo* imaging. In this case, some excellent curcumin-based fluorescent sensors have constructed.[36–38] Therefore, it is promising for the development of a new curcumin-based fluorescent sensor for H_2O_2 detection.

It has been reported that β-dicarbonyl compounds which form a rigid structure with boron trifluoride (BF_3), could enhance the fluorescence emission wavelength.[39,40] Based on this research, BF_3 was purposefully added to curcumin to amplify its conjugation effect and sequentially modulate its fluorescence properties. In the research reported in this paper, a novel curcumin-based fluorescent sensor based on **DFCB** was developed. The quenching mechanism of **DFCB** on H_2O_2 was confirmed by high resolution mass spectrometry (HRMS) analysis, ^{1}H-NMR titration and DFT calculations. The bilateral ether bond of the **DFCB** sensor would be broken in the presence of H_2O_2, which leads to a significant change of the color which can be seen by the "naked eye", and the spectral properties of the sensor. The **DFCB** sensor emitted orange fluorescence at 601 nm and exhibited a significantly quenched fluorescence response to H_2O_2. The **DFCB** sensor showed a high sensitivity and favorable selectivity for H_2O_2 in PBS solution (containing 50% CH_3CN, pH = 7.4). More importantly, the **DFCB** sensor could detect H_2O_2 in HeLa cells as well as in living zebrafish, which confirmed that the **DFCB** sensor could be used to effectively monitor exogenous and endogenous H_2O_2 in a biological system.

Results and discussion

Design and synthesis of the DFCB sensor

In this research, a new curcumin-based fluorescent sensor was constructed for H_2O_2 detection. In this sensor, the curcumin unit is used logically as a highly effective fluorescent framework due to its lipophilic long-chain conjugate. After that, boron trifluoride diethyl etherate ($BF_3{\cdot}(C_2H_5)_2O$) was introduced into the curcumin framework to form the **DFC** compound, which can produce a strong electron push–pull effect. Next, the 2-(4-bromomethylphenyl)-4,4,5,5-tetramethyl-1,3,2-doxaborolane group was introduced into the molecule and used as a recognition group for H_2O_2. As expected, the sensor exhibited a significant fluorescence emission in the PBS solution (containing 50% CH_3CN, pH = 7.4). After reaction with H_2O_2, the 2-(4-bromomethylphenyl)-4,4,5,5-tetramethyl-1,3,2-doxaborolane group of the **DFCB** sensor was selectively broken, allowing for the formation of the intermediate **DFC**, which would lead to a significantly quenched fluorescence emission. The chemical structure of the **DFCB** sensor was confirmed using ^{13}C-NMR, ^{1}H-NMR and HRMS analyses (see the ESI†).

Spectral properties of DFCB in response to H_2O_2

The optical properties of the **DFCB** sensor in the absence and presence of H_2O_2 were determined using UV-vis absorption and fluorescence spectroscopy. As shown in Fig. 1a, the **DFCB** sensor had a sharp and strong absorption band at 503 nm. After adding 300 μM H_2O_2 into the solution of the **DFCB** sensor, the absorbance at 503 nm decreased significantly, whereas a new absorption band appeared at 601 nm. At the same time, the color of the solution changed from bright orange to light blue. The previous data indicated that the **DFCB** sensor can serve as a colorimetric sensor for detecting H_2O_2. As shown in Fig. 1b, the fluorescence spectra of **DFCB** sensor had a strong fluorescence emission at 601 nm. However, after addition of 300 μM H_2O_2, the fluorescence emission of the **DFCB** sensor decreased significantly, and the color of the fluorescence changed from bright orange to colorless. The fluorescence spectral results indicated that the **DFCB**

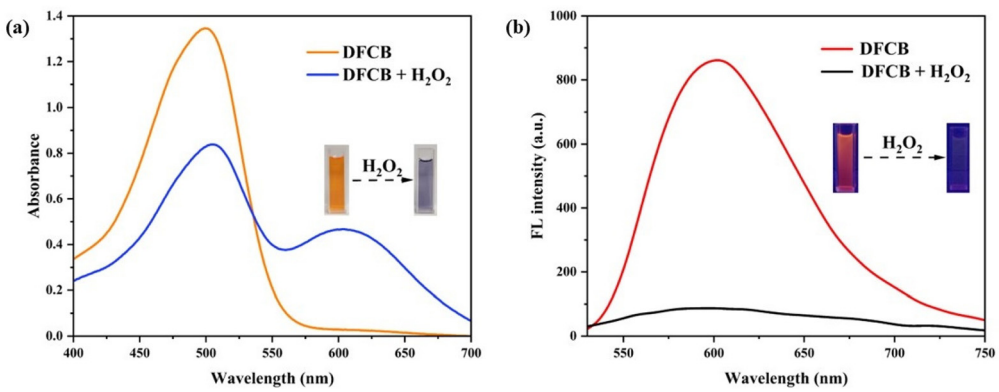

Fig. 1 (a) The UV-vis absorption, and (b) the fluorescence spectra of the **DFCB** (100 μM) sensor before and after addition of H_2O_2 (300 μM) in PBS solution (containing 50% CH_3CN, pH = 7.4). λ_{ex} = 425 nm.

sensor could be used as a turn off fluorescence sensor for H_2O_2 detection.

Sensitivity of the DFCB sensor to H_2O_2

In order to explore the sensitivity of the **DFCB** sensor for detecting H_2O_2, the UV-vis absorption and fluorescence spectra of the **DFCB** sensor in response to different concentrations of H_2O_2 were studied. As shown in Fig. 2a, with gradual addition of H_2O_2 (0–300 μM), the absorption peak of sensor **DFCB** at 503 nm weakened gradually, whereas a new UV absorption peak appeared at 601 nm and was gradually enhanced. The absorption intensity ($A_{601\ nm}/A_{503\ nm}$) of the **DFCB** sensor showed a good linear relationship with the H_2O_2 concentration (0–300 μM), and the linear regression equation was $y = 0.00469 + 0.00117x$ ($R^2 = 0.99152$). These experimental data indicated that the **DFCB** sensor could be employed for the colorimetric quantitative detection of H_2O_2.

The fluorescence spectra of the **DFCB** sensor for detecting H_2O_2 were measured. As shown in Fig. 2c, with the gradual addition of 0–300 μM H_2O_2, the fluorescence emission peak of the **DFCB** sensor at 601 nm gradually weakened, and the fluorescence intensity of the **DFCB** sensor showed a linear relationship with the concentration of H_2O_2 (0–300 μM). The linear regression equation was: $y = 829.10482 - 3.08365x$ ($R^2 = 0.99001$). According to the literature, the formula for the limit of detection was: LOD = $3\sigma/\kappa$, and the detection limit was calculated to be 1.31 μM,[11] which was comparable to that of a previously reported sensor. Based on the UV-vis absorption and fluorescence spectroscopy, the **DFCB** sensor had high sensitivity and a low detection limit for H_2O_2.

Selectivity of the DFCB sensor to H_2O_2

The selectivity and anti-interference properties of the **DFCB** sensor for the detection of H_2O_2 were measured. As shown in Fig. 3a, the fluorescence spectra of the **DFCB** sensor after the addition of different analytes (AcO^-, Ag^+, Ba^{2+}, Br^-, Ca^{2+}, Cl^-, ClO^-, ClO_4^-, Co^{2+}, CrO_7^{2-}, Cs^{2+}, Cu^{2+}, H_2O_2, $H_2PO_4^-$, Hg^{2+}, HSO_3^-, HSO_4^-, I^-, K^+, *meta*-chloroperoxybenzoic acid (MCPBA), Mg^{2+}, Mn^{2+}, Na^+, Ni^{2+}, NO_2^-, NO_3^-, $^{\bullet}OH$, $ONOO^-$, PAA, SO_4^{2-}, TBHP, Zn^{2+}). After adding these analytes, the fluorescence intensity of the **DFCB** sensor was sharply quenched after the reaction with H_2O_2. In contrast, after the addition of the other analytes, the fluorescence intensity of the **DFCB** sensor exhibited no significant changes. These data demonstrated the superior selectivity of the **DFCB** sensor to H_2O_2. The anti-interference properties of the **DFCB** sensor for detecting H_2O_2 were investigated. As shown in Fig. 3b, the fluorescence intensity of the **DFCB** sensor with H_2O_2 was not affected by the presence of other analytes. Previous results had

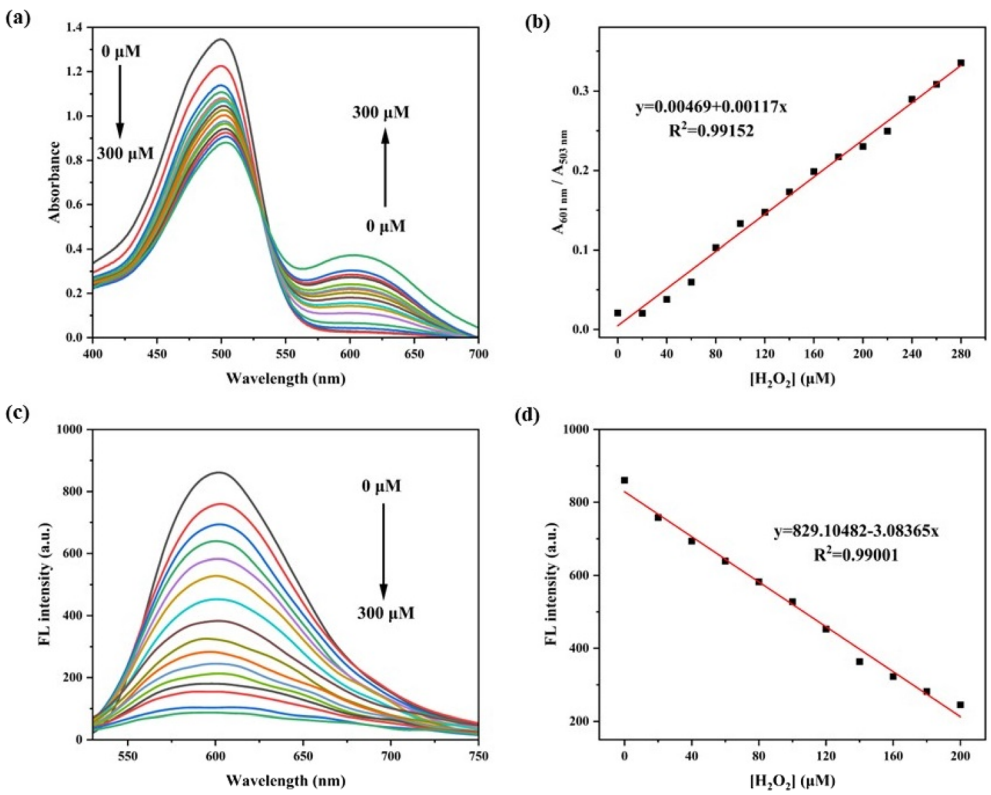

Fig. 2 (a) The UV-vis absorption spectra of the **DFCB** sensor (100 μM) with the addition of H_2O_2 (0–300 μM) in PBS buffer (containing 50% CH_3CN, pH = 7.4). (b) The linear fitting relationship between the H_2O_2 concentration and the absorption intensity ratio ($A_{601\ nm}/A_{503\ nm}$) of the **DFCB** sensor. (c) The fluorescence spectra of the **DFCB** sensor (100 μM) with the addition of H_2O_2 (0–300 μM) in PBS buffer (containing 50% CH_3CN, pH = 7.4). (d) The linear fitting relationship between H_2O_2 concentration and the fluorescence intensity of the **DFCB** sensor at 601 nm.

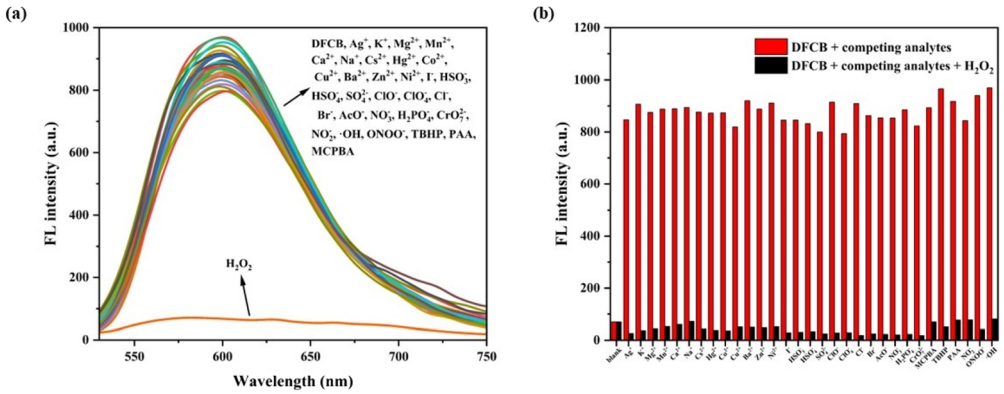

Fig. 3 (a) The fluorescence spectra of **DFCB** after the introduction of various analytes (300 μM) in PBS buffer (containing 50% CH_3CN, pH = 7.4). (b) The fluorescence intensity of the **DFCB** sensor with H_2O_2 at 601 nm in the presence of other analytes (300 μM) in PBS buffer (containing 50% CH_3CN, pH = 7.4). λ_{ex} = 425 nm.

indicated that the **DFCB** sensor had excellent selectivity and anti-interference properties for H_2O_2.

Effects of pH and response time

The pH detection range determines whether the sensor can be applied in a biological environment. As shown in Fig. 4a, the **DFCB** sensor exhibited a high fluorescence intensity at 601 nm, which indicated its good stability. When the pH was located in the range of 2–6, the **DFCB** sensor showed no remarkable fluorescence change because the H_2O_2 can react with acid to produce H_2O and O_2 in an acidic environment. However, when the pH value increased to above 7, the fluorescence emission of the **DFCB** sensor was sharply quenched, which suggested that the **DFCB** sensor had an excellent detection ability over a wide pH range, and could be applied to living organisms. The response time of the **DFCB** sensor to H_2O_2 was evaluated. As shown in Fig. 4b, after the addition of H_2O_2, the fluorescence intensity of the **DFCB** sensor dramatically decreased and reached saturation after 44 min, which suggested that the **DFCB** sensor can be employed for real-time monitoring of H_2O_2 (Table 1).

Detection mechanism

In order to demonstrate the reaction mechanism of **DFCB** to H_2O_2, HRMS analysis of the reaction product of the **DFCB** sensor with H_2O_2 was performed. As shown in Fig. 5(a), it was observed that the main molecular ion peaks were recorded at an *m*/*z* value of 439.1144, which was consistent with the stable **DFC** ($[M + Na]^+$ = *m*/*z* 439.1135). It was hypothesized that the boronate ester group of the **DFCB** sensor was oxidized and then dissociated fully to form the intermediate ($[M + K]^+$ = *m*/*z* 665.1566) in the presence of H_2O_2, followed by quinoid dissociation to form stable **DFC**. In addition, the results of the HRMS analysis confirmed that the probable peak was recorded at an *m*/*z* value of 665.1585 when about 2 eq. H_2O_2 was added. The HRMS analysis confirmed the logic of our preliminary analytical reaction mechanism.

To demonstrate the reaction mechanism between the **DFCB** sensor and H_2O_2, the ^{1}H-NMR spectra of the **DFCB** sensor after reaction with different amounts of H_2O_2 were recorded. As shown in Fig. 6, after adding H_2O_2 into the DMSO-d_6 solution of the **DFCB** sensor, the proton signal peaks (H_a) of the phenylborate groups at 1.29 ppm disappeared with the

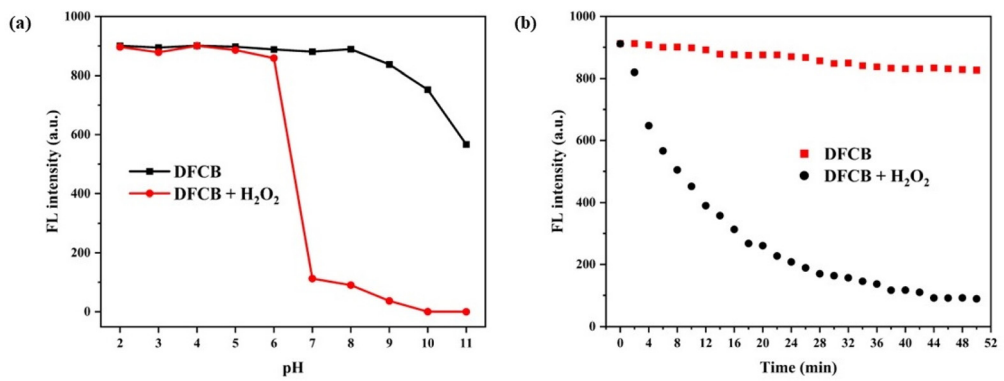

Fig. 4 (a) Fluorescence intensity of the **DFCB** sensor (100 μM) at different pH values in the absence and presence of H_2O_2 (300 μM) in PBS buffer (containing 50% CH_3CN, pH = 7.4). (b) Response time of the **DFCB** sensor (100 μM) to H_2O_2 (300 μM) in PBS buffer (containing 50% CH_3CN, pH = 7.4).

Table 1 Comparison of other fluorescence sensors reported for specific detection of H_2O_2

Sensors	Response time	Detection limit (μM)	Linear range	pH range	Application
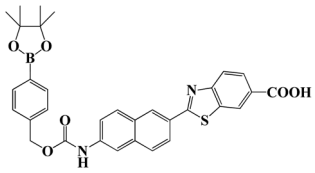 Ref. 41	120 min	4.0	0–1 μM	Not mentioned	Living mice
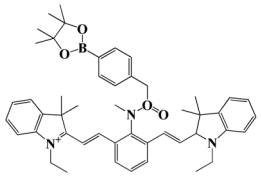 Ref. 42	70 min	20	0–10 μM	48	Living mice
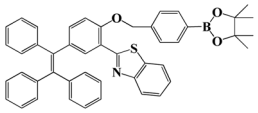 Ref. 43	180 min	6.0	0–100 μM	5–8	Living cells
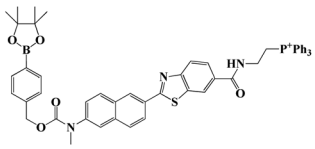 Ref. 44	60 min	4.6	0–1 mM	4–11	Living cells
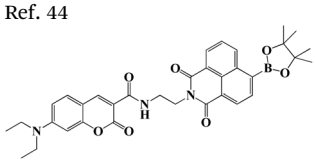 Ref. 45	60 min	1.35	0–200 μM	4–10	Living cells and living zebrafish
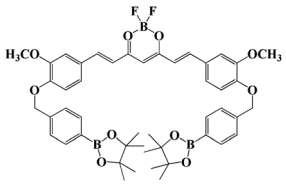 This work	44 min	1.31	0–300 μM	6–11	Living cells and living zebrafish

increase of the H_2O_2 equivalent. At the same time, the proton signal peaks (H_b) of the methylene units at 5.5 gradually disappeared, which indicated that the boronate ester group of the **DFCB** sensor can react with H_2O_2 and was then removed. Based on HRMS analysis and ^{1}H-NMR titration, the sensing mechanism of **DFCB** on H_2O_2 was selective boron oxidation which formed the intermediate, and the elimination reactions to release **DFC**, which might break the original structure of the sensor and would result in a significant weakening of the fluorescence emission at 601 nm.

The DFT calculation was carried out using the Gaussian 09 program to further reveal the optical changes of the **DFCB** sensor before and after the reaction with H_2O_2. Fig. 7 shows the spatial distribution and energy orbitals of the lowest unoccupied molecular orbital (LUMO) and the highest occupied molecular orbital (HOMO) of the **DFCB** sensor and the **DFC** compound. The LUMO and HOMO of the **DFCB** sensor were mainly distributed on the fluorine-boron core, the C=C bond, and the benzene ring, indicating the weak charge transfer effect of the **DFCB** sensor. However, the LUMO of the **DFCB** sensor was distributed on the fluorine-boron core and the C=C bond, whereas its HOMO was distributed on the phenol group, which would activate the charge transfer effect of the **DFCB** sensor after reaction with H_2O_2, and then it led to a red-shifted absorption spectra.

Imaging of DFCB in HeLa cells

The use of the **DFCB** sensor for imaging H_2O_2 was investigated in living HeLa cells. Prior to the cell fluorescence imaging experiment, the cytotoxicity of the **DFCB** sensor was measured. As shown in Fig. S7 (ESI†), the **DFCB** sensor (0–4 μM) had no significant effect on the survival rate of the HeLa cells, and the cell survival rate was over 90%. This indicated that the **DFCB**

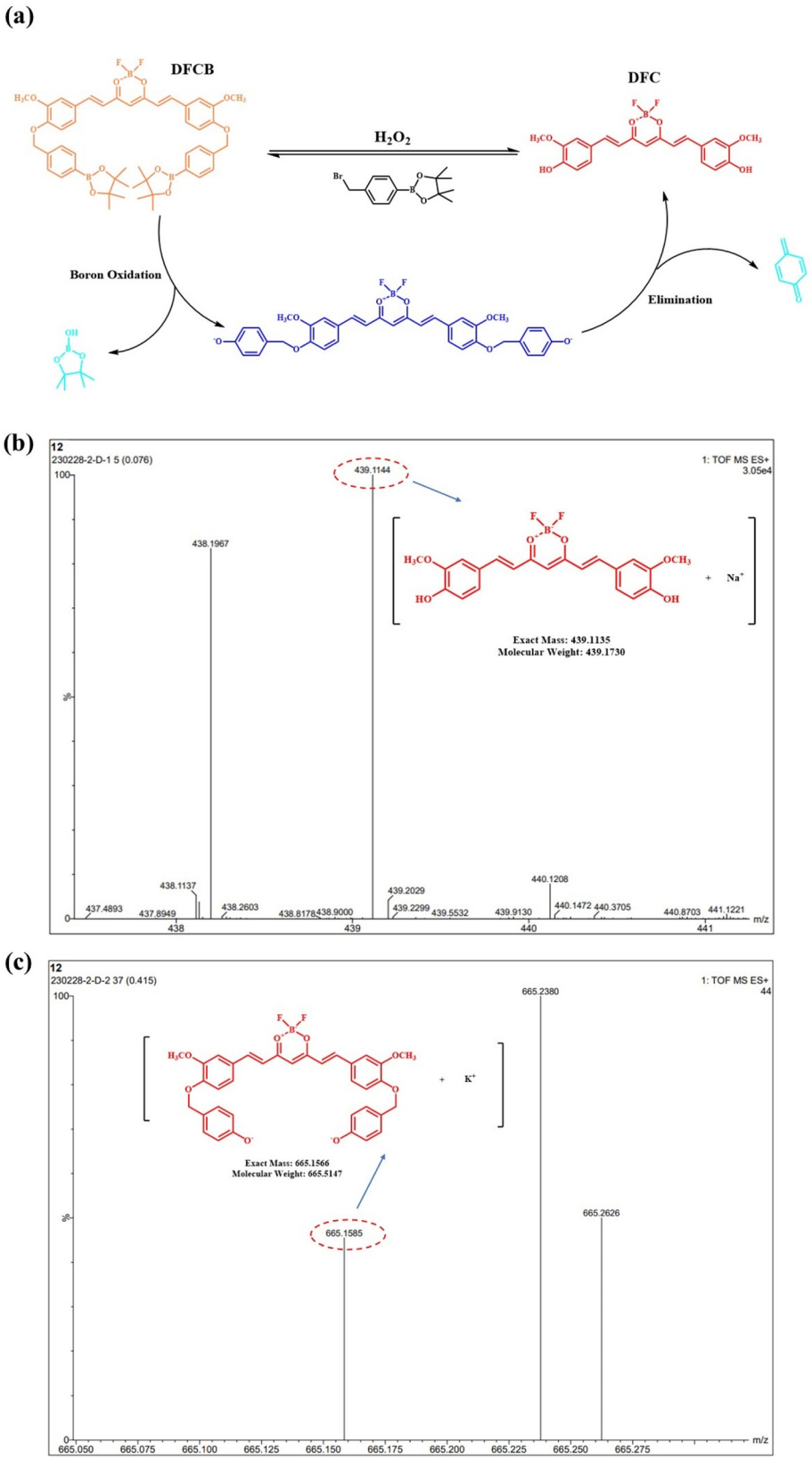

Fig. 5 (a) The proposed sensing mechanism of **DFCB** with H_2O_2. (b) The HRMS spectra of the reaction of the **DFCB** sensor with 5 eq. H_2O_2. (c) The HRMS spectra of the reaction of the **DFCB** sensor with 2 eq. H_2O_2.

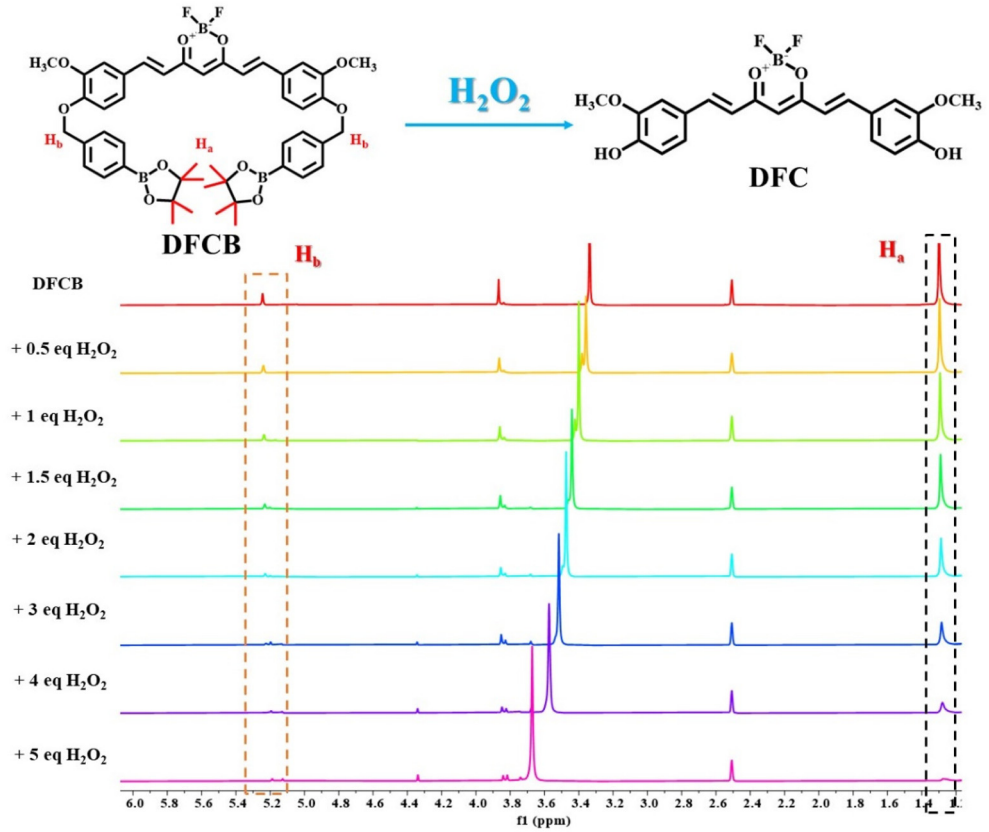

Fig. 6 The ^{1}H-NMR spectra of the **DFCB** sensor before and after the reaction with different amounts of H_2O_2.

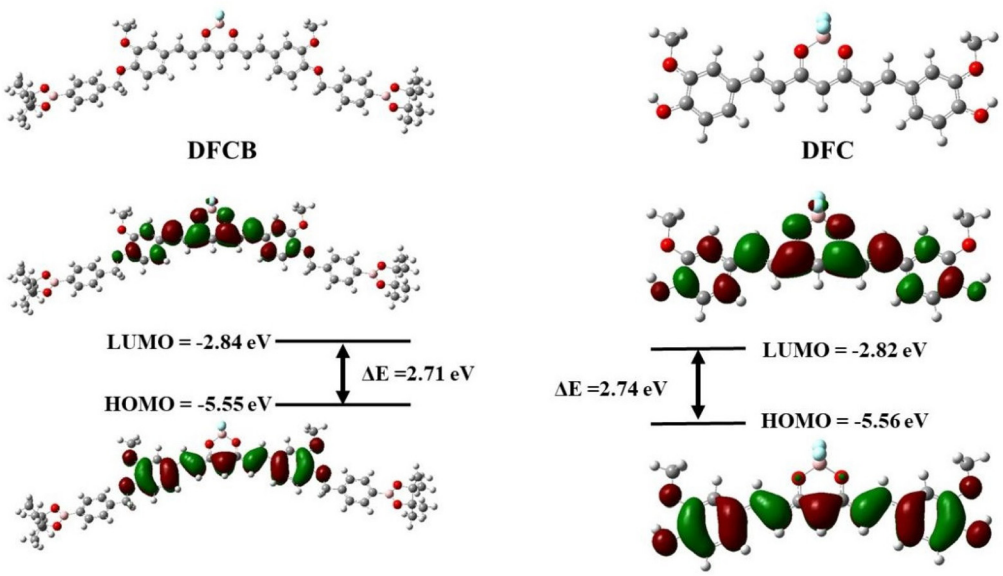

Fig. 7 Optimized geometric configurations and frontier molecular orbitals of the **DFCB** sensor and the **DFC** intermediate.

sensor was less cytotoxic to cells and that it could be applied in the cell imaging experiment.

Furthermore, the **DFCB** sensor was used for fluorescence imaging in living cells. As shown in Fig. 8, the control cells showed no observable fluorescence emission. With the addition of the **DFCB** sensor, the HeLa cells emitted an orange fluorescence, which demonstrated that the sensor had good cell permeability and biocompatibility. After further incu-

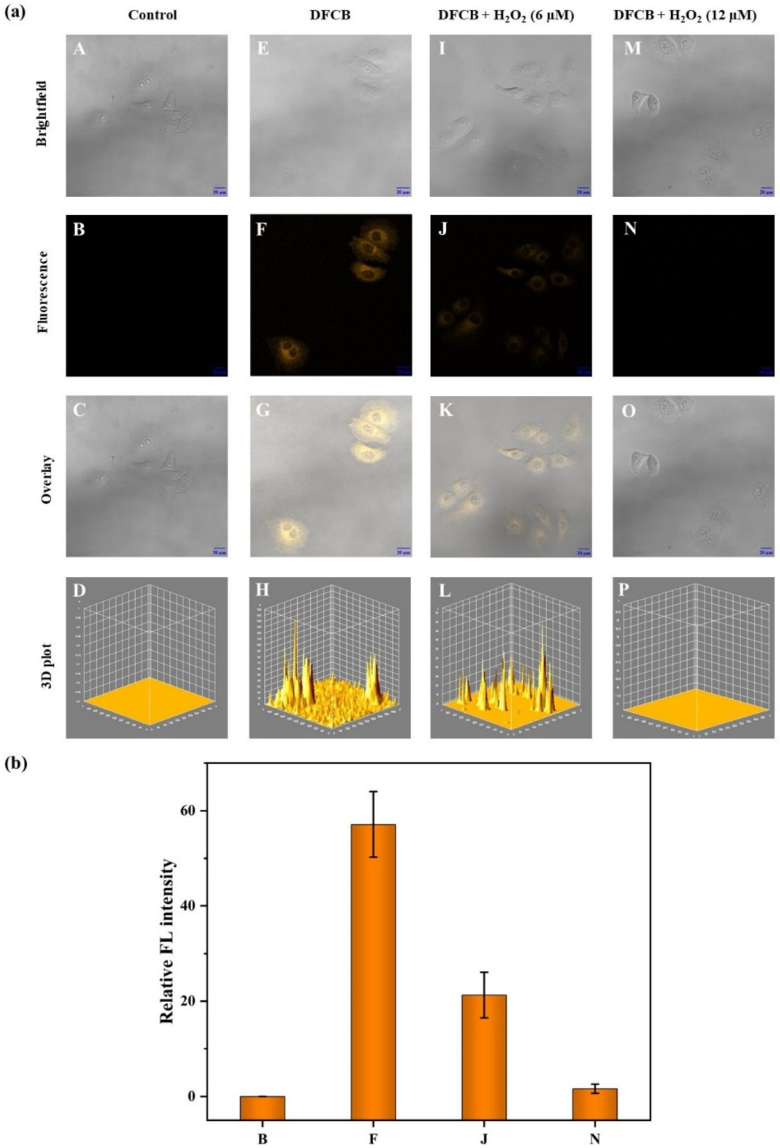

Fig. 8 (a) Imaging of H_2O_2 in HeLa cells: (A–C) only the HeLa cells were cultured for 1 h; (E–G) HeLa cells supplemented with the **DFCB** sensor (4 μM) were cultured for 1 h; (I–K) HeLa cells supplemented with the **DFCB** sensor (4 μM) and H_2O_2 (6 μM) were cultured for 30 min; and (M–O) HeLa cells were cultured with the **DFCB** sensor (4 μM) and H_2O_2 (12 μM) for 1 h. (D, H, L and P) are the corresponding 3D surface plots of the fluorescence images. (b) Quantitative intensity obtained from the fluorescent images of the HeLa cells.

bation with increasing concentrations of H_2O_2 (6 and 12 μM), the fluorescence intensity of the cells gradually decreased and was completely quenched. The 3D surface plot and the relative fluorescence intensity were calculated to support the fluorescence quenching effect in living cells, which demonstrated that the **DFCB** sensor could be utilized for imaging exogenous H_2O_2 *in vitro*.

The fluorescence labeling, with endogenous H_2O_2, was carried out in HeLa cells using the **DFCB** sensor. As shown in Fig. 9, in the presence of the free **DFCB** sensor (4 μM), there was significant fluorescence emission in the HeLa cells. Since phorbol myristate acetate (PMA, a ROS stimulant) could promote endogenous H_2O_2 production, the HeLa cells displayed quenching which was supplemented with PMA (1 μg ml^{-1}), and subsequently the cells were cultured for 30 min. If the cells were cultured with PMA for 60 min, the fluorescence intensity decreased further, which indicated that the **DFCB** sensor could detect endogenous H_2O_2. In addition, to verify that the endogenous H_2O_2 production could cause the fluorescence quenching in the cells, the PMA-stimulated cells were further supplemented with *N*-acetyl-L-cysteine (NAC, a ROS scavenger, 1 mM) and then stained with the **DFCB** sensor. From Fig. 9(b) it was concluded that the average fluorescence intensity was enhanced after the removal of the endogenous H_2O_2 from the HeLa cells. The previously described experimental imaging data confirmed the excellent imaging ability of the

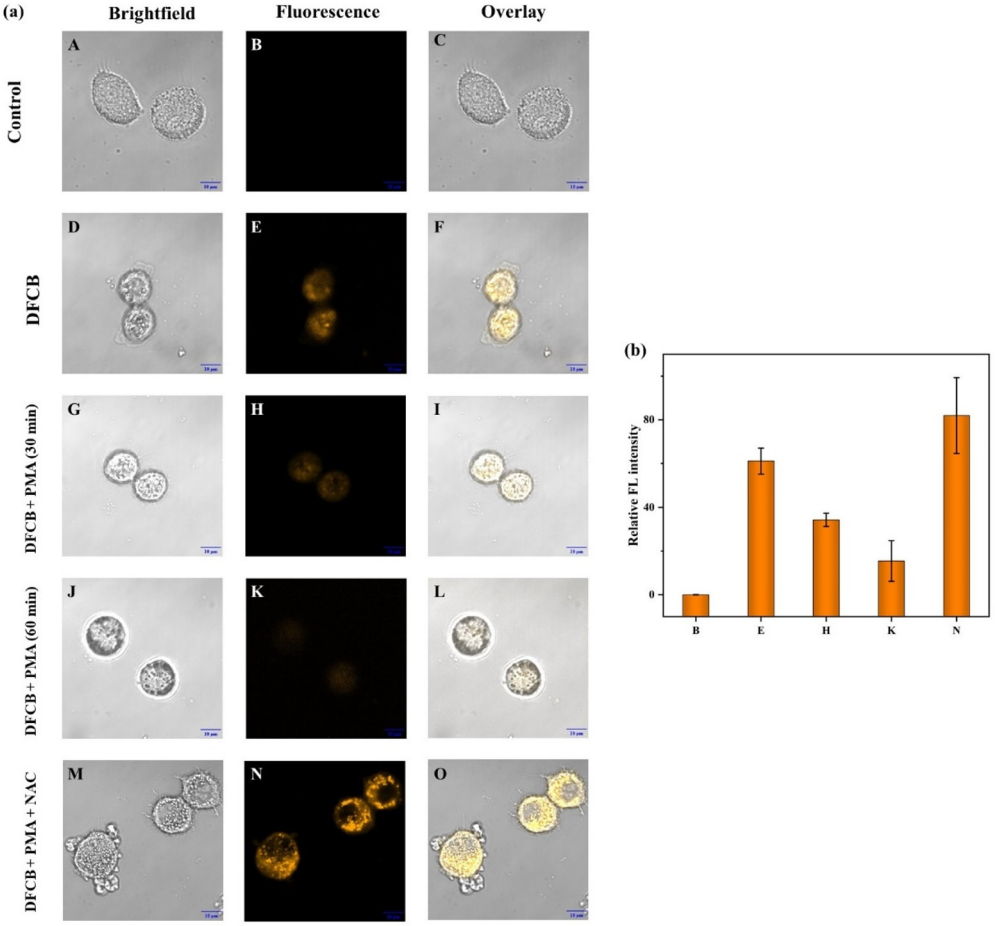

Fig. 9 (a) Imaging of H_2O_2 in HeLa cells: (A–C) HeLa cells alone were cultured for 1 h and acted as the control; (D–F) HeLa cells supplemented with the **DFCB** sensor (4 μM) were cultured for 1 h; (G–I) the HeLa cells supplemented with PMA (1 μg ml^{-1}) were cultured for 30 min; (J–L) subsequently, the HeLa cells supplemented with PMA (1 μg ml^{-1}) were cultured for 60 min; and (M–O) the HeLa cells were cultured with PMA (1 μg ml^{-1}) and then incubated with NAC (1 mM), followed by staining with the **DFCB** sensor (4 μM) for 1 h. (b) The quantitative intensity was obtained from the fluorescent images of the HeLa cells.

DFCB sensor for generating endogenous H_2O_2. In addition, the untreated HeLa cells were selected as the control group. Significant fluorescence emission could not be observed in the cells due to the absence of the **DFCB** sensor, and these experimental data confirmed that the **DFCB** sensor could be used to monitor endogenous H_2O_2 production in living cells. All these cellular experiments confirmed that the **DFCB** sensor could image endogenous H_2O_2 in living cells.

Bioimaging in zebrafish

The **DFCB** sensor was further used to detect H_2O_2 *in vivo*. As shown in Fig. 10, zebrafish treated with the **DFCB** sensor (4 μM) exhibited an intense orange fluorescence, suggesting that the **DFCB** sensor possessed excellent cell permeability. However, the fluorescence intensity of the **DFCB** sensor gradually decreased until it was completely quenched by the increase of H_2O_2 concentration (6 and 12 μM). Furthermore, the fluorescence imaging phenomenon in living zebrafish was supported by the 3D surface and the relative fluorescence intensity plots. The previous experimental results showed that the **DFCB** sensor can detect exogenous H_2O_2 in organisms.

As shown in Fig. 11, the zebrafish incubated with the **DFCB** sensor (4 μM) emitted an orange fluorescence unlike the control group, which confirmed that zebrafish cannot emit fluorescence by themselves. With the addition of PMA (1 μg ml^{-1}) for different times, the emission fluorescence of the **DFCB** sensor in zebrafish was gradually quenched, which indicated that the PMA supplement could stimulate the production of endogenous H_2O_2 in zebrafish. Compared with the zebrafish with the **DFCB** sensor, the fluorescence intensity was stronger in the zebrafish which was treated with NAC (1 mM) and then cultured with the **DFCB** sensor. These experimental results confirmed that the **DFCB** sensor had good potential for use in biological imaging and in the detection of endogenous H_2O_2. In addition, the relative fluorescence intensity chart was used to support the biological imaging experiments. These experimental data indicated that the **DFCB** sensor can detect exogenous and endogenous levels of H_2O_2 in biological systems.

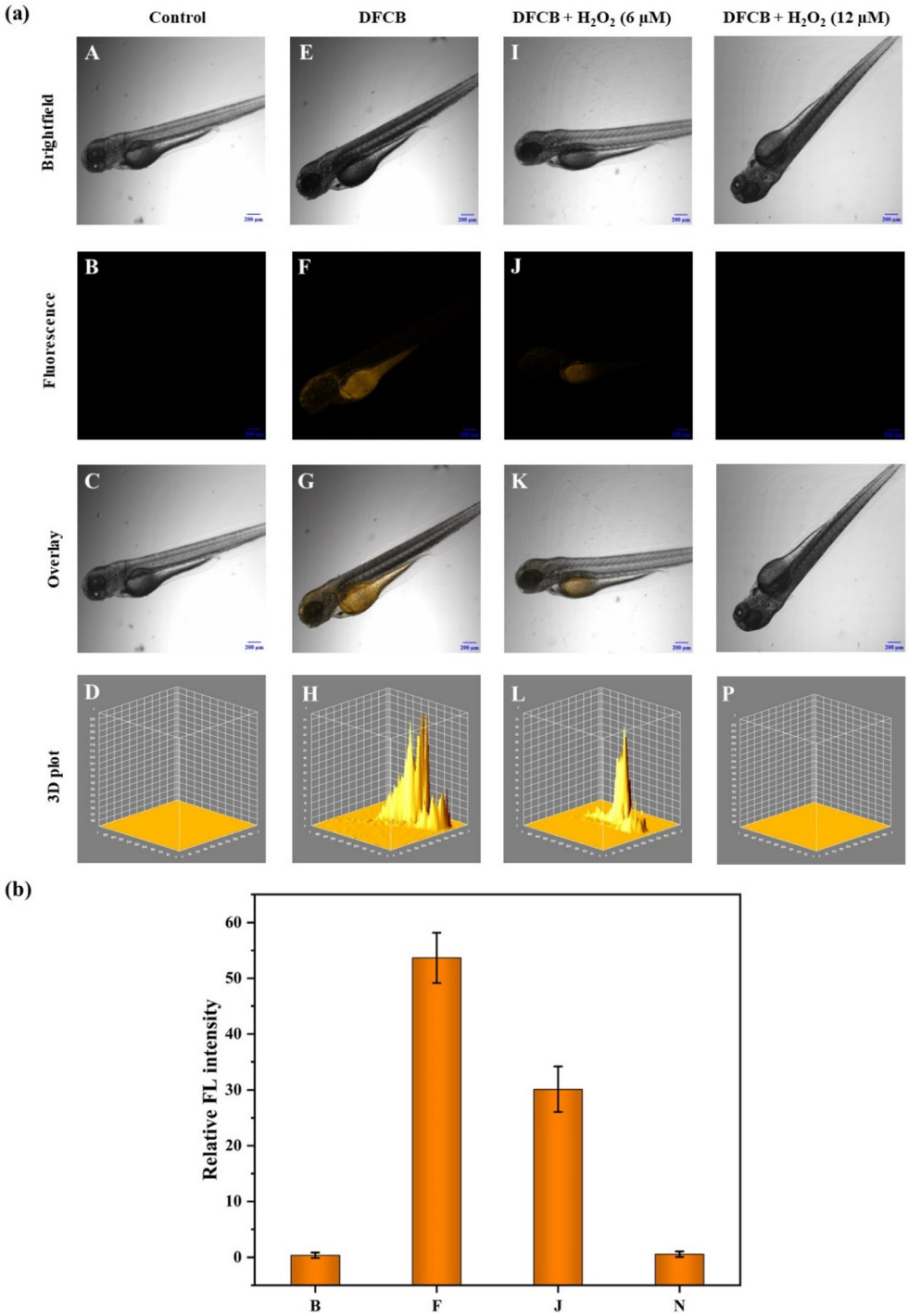

Fig. 10 (a) Imaging of H_2O_2 in zebrafish: (A–C) zebrafish alone were cultured for 1 h and acted as the control; (E–G) zebrafish supplemented with the **DFCB** sensor (4 μM) were cultured for 1 h; (I–K) zebrafish supplemented with the **DFCB** sensor (4 μM) and H_2O_2 (6 μM) were cultured for 30 min; and (M–O) zebrafish were cultured with the **DFCB** sensor (4 μM) and H_2O_2 (12 μM) for 1 h. (D, H, L and P) are the corresponding 3D surface plots of the fluorescence images. (b) Quantitative intensity was obtained from fluorescent images of the zebrafish.

Experiments

Instruments and materials

The chemical reagents used in the experiments are normally available commercially and were used directly. Curcumin was purchased from the Shanghai Titan Technology Company. The $BF_3{\cdot}(C_2H_5)_2O$ was obtained from the Shanghai Lingfeng Chemical Reagent Company. The 2-(4-bromomethylphenyl)-4,4,5,5-tetramethyl-1,3,2-doxaborolane was obtained from the Shanghai Haohong Biomedical Technology Company. The

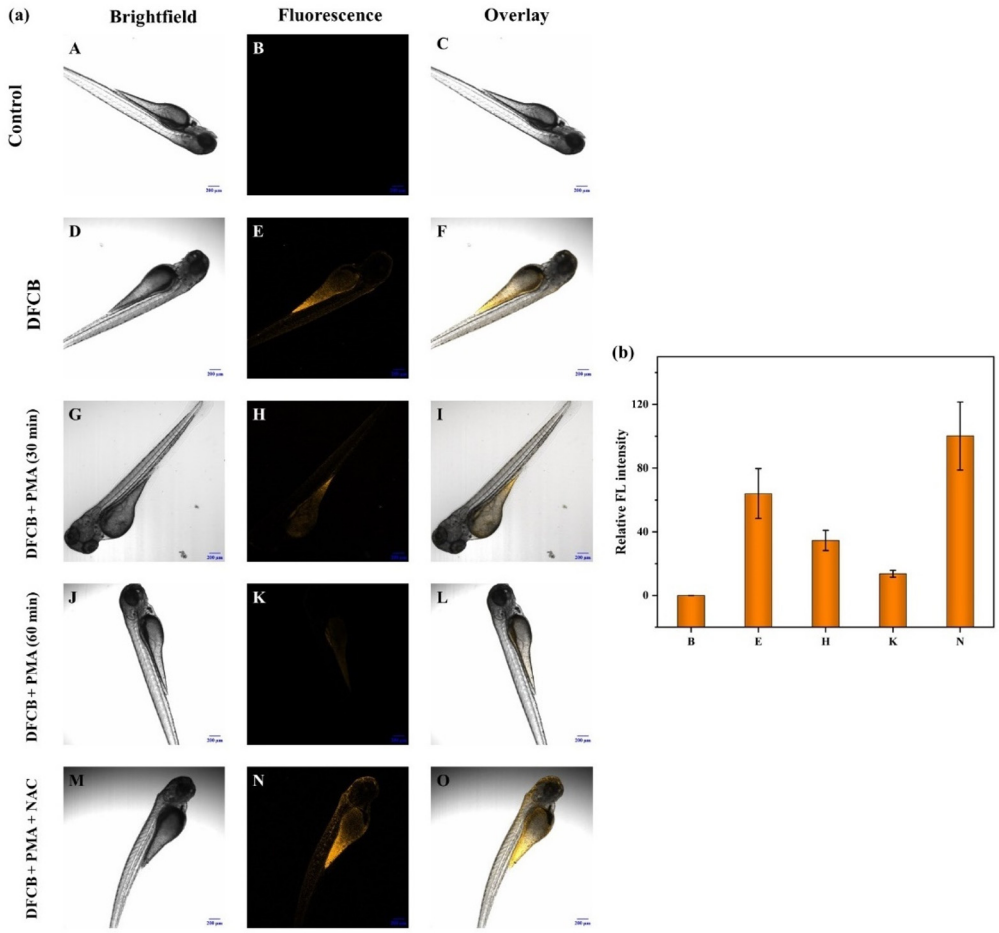

Fig. 11 (a) The imaging of H_2O_2 in zebrafish: (A–C) zebrafish alone were cultured for 1 h; (D–F) zebrafish supplemented with the **DFCB** sensor (4 μM) were cultured for 1 h; (G–I) zebrafish supplemented with PMA (1 μg ml^{-1}) were cultured for 30 min; (J–L) subsequently, the zebrafish supplemented with PMA (1 μg ml^{-1}) were cultured for 60 min; and (M–O) the zebrafish were cultured with PMA (1 μg ml^{-1}) and then incubated with NAC (1 mM), followed by staining with the **DFCB** sensor (4 μM) for 1 h. (b) Quantitative intensity obtained from fluorescent images of zebrafish.

^{1}H-NMR and ^{13}C-NMR spectra were recorded on a AV-600 NMR spectrometer (Bruker). The HRMS was carried out on a JMS-800D mass spectrometer (Jeol). The UV-vis absorption spectra were recorded on a UV-2450 spectrometer (Shimadzu). The fluorescence emission spectra were recorded using a LS55 fluorescence spectrometer (PerkinElmer).

Synthesis of compound DFC

Curcumin (1 mmol) was dissolved in 30 mL of CH_2Cl_2 at ambient temperature, and $BF_3{\cdot}(C_2H_5)_2O$ (2.4 mmol) was added dropwise. The reaction was continued for 5 h, and monitored with thin layer chromatography. After concentrating and removing half of the solvent, the reaction mixture was placed in a refrigerator for crystallization to take place. The red solid product **DFC** was obtained by filtering, washing with CH_2Cl_2, and drying, with a yield of 98%. ^{1}H-NMR (600 MHz, DMSO-d_6) δ: 10.09 (s, 2H), 7.92 (d, J = 15.5 Hz, 2H), 7.47 (s, 2H), 7.34 (d, J = 10.3 Hz, 2H), 7.01 (d, J = 15.6 Hz, 2H), 6.87 (s, 2H), 6.45 (s, 1H), 3.85 (s, 6H). ^{13}C-NMR (151 MHz, DMSO-d_6) δ: 178.89, 151.52, 148.35, 147.14, 126.16, 125.44, 118.03, 116.13, 112.56, 101.29, 55.94. HRMS (m/z): $[M + H]^+$ calcd for $C_{21}H_{19}BO_6F_2Na + H^+$, 439.1140; found, 439.1141.

Synthesis of the DFCB sensor

The **DFC** (1 mmol) and 2-(4-bromomethylphenyl)-4,4,5,5-tetramethyl-1,3,2-doxaborolane (2.4 mmol), and K_2CO_3 (2.4 mmol) were dissolved in 8 mL of CH_3CN, and the reaction mixture was then refluxed for 6 h. The reaction mixture was kept in cryogenic refrigerator overnight, and the brown precipitate was filtered to obtain the crude **DFCB**. The crude **DFCB** was dissolved in ethyl acetate, and washed with deionized water until the pH became neutral. After drying with $MgSO_4$, followed by filtration, and distillation of the solvent, the **DFCB** was finally obtained, with a yield of 53% (Scheme 1). ^{1}H-NMR (600 MHz, DMSO-d_6) δ: 7.96 (d, J = 15.6 Hz, 2H), 7.70 (d, J = 7.6 Hz, 4H), 7.53 (s, 2H), 7.44 (dd, J = 17.0, 8.1 Hz, 6H), 7.17–7.07 (m, 4H), 6.52 (s, 1H), 5.23 (s, 4H), 3.86 (s, 6H), 1.29 (s, 24H). ^{13}C-NMR (151 MHz, DMSO-d_6) δ: 179.43, 158.87, 158.65, 158.42, 158.20, 151.59, 149.70, 147.12, 144.36, 140.22, 134.91, 127.77, 127.32, 125.34, 124.51, 119.42, 117.70, 115.75, 113.67, 111.96, 84.00,

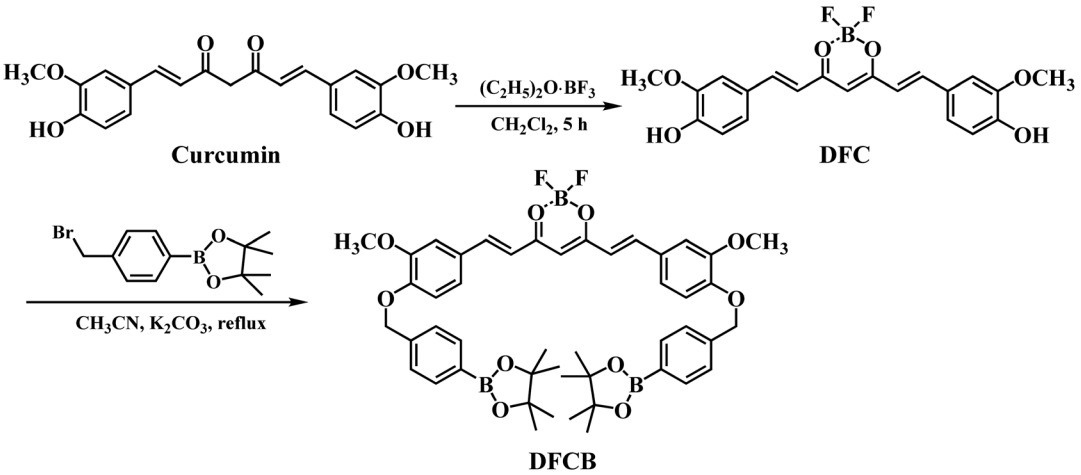

Scheme 1 The synthesis route for the **DFCB** sensor.

70.03, 56.12, 24.95. HRMS (*m*/*z*): $[M + H]^+$ calcd for $C_{47}H_{53}B_3O_{10}F_2Na + H^+$, 871.3784; found, 871.3794.

Spectral measurements

The stock solution of **DFCB** (1 mM) was prepared in CH_3CN. The stock solutions of different metal ions (10 mM) (Ag^+, Ba^{2+}, Ca^{2+}, Co^{2+}, Cs^{2+}, Cu^{2+}, Hg^{2+}, K^+, Mg^{2+}, Mn^{2+}, Na^+, Ni^{2+}, Zn^{2+}), anions (AcO^-, Br^-, Cl^-, ClO^-, ClO_4^-, CrO_7^-, $H_2PO_4^-$, HSO_3^-, HSO_4^-, I^-, NO_3^-, NO_2^-, SO_4^{2-}) and ROS (MCPBA, $^{\bullet}OH$, $ONOO^-$, PAA, TBHP) were prepared in deionized water. The UV-vis absorption and fluorescence spectra of the samples were recorded in PBS solution (50% CH_3CN, pH = 7.4) at room temperature. For the fluorescence spectroscopy measurements, the excitation wavelength was λ_{ex} = 425 nm, and the slit width was $\lambda_{ex}/\lambda_{em}$ = 5 nm/5.5 nm.

HeLa cell and zebrafish imaging

The HeLa cells were cultured in DMEM containing 10% fetal bovine serum (FBS) with 5% CO_2 at 37 °C. Next, the cells were divided into four groups. Except for group 1, the other cells from groups 2 to 4 were incubated in 4 μM **DFCB** solution for 1 h at 37 °C, and then incubated with different concentrations of H_2O_2 (0, 6, 12 μM) for another 30 min. Fluorescence images of the HeLa cells were recorded using a laser confocal fluorescence microscope in the orange channel (λ_{ex} = 405 nm, λ_{em} = 450–650 nm).

Four-day-old zebrafish were randomly divided into three groups. Each group was incubated with 4 μM of the **DFCB** sensor for 30 min, and then incubated with different concentrations of H_2O_2 (0 μM, 6 μM, and 12 μM) for 44 min. After washing the zebrafish three times with the PBS solution, the fluorescence images of the zebrafish were obtained using a laser confocal fluorescence microscope in the orange channel (λ_{ex} = 405 nm, λ_{em} = 450–650 nm).

Conclusions

In summary, a new curcumin-based fluorescent **DFCB** sensor was designed and synthesized for use in H_2O_2 detection. The **DFCB** sensor emitted an intense orange fluorescence and exhibited a significant quenched fluorescence response to H_2O_2. The color of the **DFCB** sensor solution changed from orange to blue in the presence of H_2O_2, when the solution was viewed with the naked eye. The **DFCB** sensor could selectively detect H_2O_2 and showed a good anti-interference performance. Moreover, the **DFCB** sensor exhibited the advantages of a low detection limit (1.31 μM), wide linear range (0–300 μM), and broad pH detection range (6–11). Furthermore, the **DFCB** sensor with low cytotoxicity and good biocompatibility was successfully used for imaging endogenous and exogenous H_2O_2 in living HeLa cells, as well as in living zebrafish. We predict that the results of this research will have the potential to be used in future for monitoring the physiological and pathological effects of H_2O_2 *in vivo*.

Author contributions

Wenhao Du: investigation, methodology and writing – original draft. Zheyu Shen: formal analysis. Yueying Liang: software. Shuai Gong: investigation. Zhiyuan Meng: software. Mingxing Li: data curation. Zhonglong Wang: writing – review and editing. Shifa Wang: project administration.

Ethics declarations

Ethics approval

All the animal procedures were performed in accordance with the Guidelines for Care and Use of Laboratory Animals of Nanjing University and approved by the Animal Ethics Committee of China.

Conflicts of interest

The authors declare that they have no conflict of interest.

Acknowledgements

The authors wish to thank the National Natural Science Foundation of China (Grant No. 32071707 and 32101466) and the Natural Science Foundation of Jiangsu Province (Grant No. BK20210624) for their financial support for this research.

References

1 X. Li, N. Gao, C. Liu, M. Yu, X. Rong, Y. Zhang, M. Su, X. Wang, H. Zhu, K. Wang, Y. Liu, W. Sheng and B. Zhu, *Sens. Actuators, B*, 2022, **353**, 131051.
2 X. Zhang, L. Zhang, X. Y. Cheng, S. D. Liu, S. J. Fang, L. W. Zhang, X. Y. Wang and L. X. Chen, *Sens. Actuators, B*, 2022, **366**, 131982.
3 Y. Huang, L. Yu, P. P. Lu, Y. H. Wei, L. L. Fu, J. J. Hou, Y. Q. Wang, X. Y. Wang and L. X. Chen, *J. Hazard. Mater.*, 2022, **424**, 127425.
4 Y. Q. Shi, Q. C. Wu, W. T. Li, L. Lin, F. F. Qu, C. J. Shen, Y. Z. Wei, P. C. Nie, Y. He and X. P. Feng, *J. Hazard. Mater.*, 2022, **432**, 128605.
5 Q. Xu, Y. Y. Tang, P. D. Zhu, W. Y. Zhang, Y. Q. Zhang, O. S. Solis, T. S. Hu and J. C. Wang, *Nanoscale*, 2022, **14**, 13771–13778.
6 Y. Wu, Z. Y. Li and Y. M. Shen, *ACS Omega*, 2019, **4**, 16242–16246.
7 Z. L. Wang, Y. Zhang, J. Song, M. X. Li, Y. Q. Yang, X. Xu, H. J. Xu and S. F. Wang, *Sens. Actuators, B*, 2019, **284**, 148–158.
8 J. Q. Xu, J. S. Guo, K. F. Xie, M. J. Gao, R. Wei, Z. H. Xin and Y. F. Kang, *Dyes Pigm.*, 2022, **204**, 110437.
9 X. L. Liu, M. D. Yan, Z. G. Chen, B. X. Zhang, N. C. Yao, S. Zhao, X. X. Zhao, T. Zhang and G. F. Hai, *Spectrochim. Acta, Part A*, 2023, **286**, 121955.
10 M. Chen, Z. H. Liang, G. L. Zeng, Y. Wang, Z. H. Mai, X. Y. Chen, G. Wu and T. S. Chen, *Dyes Pigm.*, 2022, **198**, 109995.
11 L. Q. Li, M. H. Zheng, X. Y. Yan, H. Huang, S. X. Cao, K. M. Liu and J. B. Liu, *J. Photochem. Photobiol., A*, 2022, **432**, 114069.
12 T. Ma, K. Fu, Z. C. Li, C. C. Yuan and W. B. Ma, *Spectrochim. Acta, Part A*, 2022, **276**, 121218.
13 M. X. Wang, F. Zhang, C. Q. Wang, N. Yin, Y. T. Wang, G. X. Qin, Q. L. Xu, J. H. Gong, H. Z. Liu and X. R. Duan, *Anal. Chem.*, 2022, **94**, 5962–5969.
14 Y. Q. Li, Y. Zhou, J. N. Lei, Q. J. Lu, X. Qin, Q. Xu, Y. Q. Wang, C. Y. Wu, Z. Yang and B. S. He, *J. Mol. Struct.*, 2023, **1271**, 134042.
15 Y. Fang, J. Wang, H. Yu, Q. Zhang, S. J. Chen, K. P. Wang and Z. Q. Hu, *Sens. Actuators, B*, 2022, **371**, 132514.
16 Y. Tian, S. Y. Liu, W. W. Cao, P. Wu, Z. M. Chen and H. Xiong, *Anal. Chem.*, 2022, **94**, 11321–11328.
17 M. Chen, Z. H. Liang, X. H. Fan, R. M. Qu, H. H. Wang and T. S. Chen, *Spectrochim. Acta, Part A*, 2022, **276**, 121163.
18 L. Guo, S. Chen, Y. L. Yu and J. H. Wang, *Anal. Chem.*, 2021, **93**, 16240–16247.
19 M. R. Li, B. W. Wang, J. Y. Liu, Z. Z. Zhang, L. G. Chen, Y. Li and X. L. Yan, *Anal. Chem.*, 2022, **94**, 9732–9739.
20 K. Yin, F. B. Yu, D. Y. Liu, Z. H. Xie and L. X. Chen, *Sens. Actuators, B*, 2016, **223**, 799–805.
21 Z. Y. Zhang, Z. P. Chen, F. B. Cheng, Y. W. Zhang and L. X. Chen, *Biosens. Bioelectron.*, 2017, **89**, 932–936.
22 X. Wang, Q. Ding, Y. Tian, W. Wu, F. D. Che, P. Li, W. Zhang, W. Zhang and B. Tang, *Chem. Commun.*, 2022, **58**, 6320–6323.
23 J. K. Liang, H. Li, J. R. Wang, H. L. Yu and Y. He, *Anal. Chem.*, 2020, **92**, 6548–6554.
24 S. Wang, Y. Zhang, T. R. Wang, Y. J. Liu, S. L. Shen and X. Q. Cao, *Spectrochim. Acta, Part A*, 2022, **266**, 120435.
25 Y. Hua, Y. J. Shang, M. J. Gao, J. Li and Y. F. Kang, *Spectrochim. Acta, Part A*, 2022, **265**, 120320.
26 X. D. Zeng, C. Jiang, Q. Zhang, D. K. Chai, M. S. Ma, J. Chen and Z. G. Liu, *J. Lumin.*, 2021, **240**, 118422.
27 J. Su, S. P. Zhang, C. R. Wang, M. Li, J. J. Wang, F. Su and Z. J. Wang, *ACS Omega*, 2021, **6**, 14819–14823.
28 L. L. Xu, Y. Zhang, L. H. Zhao, H. Han, S. Q. Zhang, Y. B. Huang, X. H. Wang, D. Q. Song, P. Y. Ma, P. Ren and Y. Sun, *Talanta*, 2021, **233**, 122578.
29 G. Q. Yang, T. Zhu, D. Wang, Z. J. Liu, R. L. Zhang, G. M. Han, X. H. Tian, B. H. Liu, M. Y. Han and Z. P. Zhang, *Chem. Commun.*, 2021, **57**, 6628–6631.
30 R. R. Zhou, Q. Y. Peng, D. Wan, C. Yu, Y. Zhang, Y. Hou, Q. Luo, X. Li, S. H. Zhang, L. Xie, P. H. Ou and Y. B. Peng, *RSC Adv.*, 2021, **11**, 24032–24037.
31 Y. M. Hao, H. P. Wang, Z. H. Wang, W. J. Dong, Q. Hu, S. M. Shuang, C. Dong and X. J. Gong, *Mikrochim. Acta*, 2021, **188**, 16.
32 X. H. Pan, Y. H. Zhao, T. T. Cheng, A. S. Zheng, A. B. Ge, L. X. Zang, K. H. Xu and B. Tang, *Chem. Sci.*, 2019, **10**, 8179–8186.
33 Z. W. Gan, T. Zhang, X. X. An, Q. Tan, S. J. Zhen, Y. M. Hu and X. L. Hu, *Microchem. J.*, 2022, **182**, 107939.
34 H. Yang, C. Yu, Z. Yin, P. Guan, S. Jin, Y. Wang and X. Feng, *J. Sci. Food Agric.*, 2022, **103**, 1550–1560.
35 H. L. Dong, P. Wang, Z. Y. Yang, R. Li, X. L. Xu and J. Shen, *Ultrason. Sonochem.*, 2022, **90**, 106188.
36 H. Li, T. Wang, J. Q. Su and P. V. Meeren, *Food Hydrocolloids*, 2022, **133**, 108020.
37 J. P. Hu, Y. L. Wang, T. Y. Shao, G. C. Lian, K. B. Hu, Y. Liu, M. Zhou, X. P. Wang, L. Z. Huang, X. L. Meng and G. F. Jin, *Arabian J. Chem.*, 2022, **15**, 104087.
38 S. Kang, B. Y. Park, S. Lee, N. Lee and M. S. Han, *Analyst*, 2021, **146**, 463–470.
39 Q. Jiang, Z. L. Wang, M. X. Li, J. Song, Y. Q. Yang, X. Xu, H. J. Xu and S. F. Wang, *Tetrahedron Lett.*, 2020, **61**, 152103.

40 Y. Gao, M. X. Li, X. C. Tian, S. Gong, Y. Zhang, Y. Q. Yang, Z. L. Wang and S. F. Wang, *Microchem. J.*, 2022, **169**, 106631.
41 C. S. Lim, M. Y. Cho, M. Y. Park and H. M. Kim, *ChemistryOpen*, 2017, **7**, 53–56.
42 R. F. Xu, Y. Wang, H. Y. You, L. W. Zhang, Y. Q. Wang and L. X. Chen, *Analyst*, 2019, **144**, 2556–2564.
43 Y. Liu, J. Nie, J. Niu, F. F. Meng and W. Y. Lin, *Sci. Rep.*, 2017, **7**, 7293.
44 G. Masanta, C. H. Heo, C. S. Lim, S. K. Bae, B. R. Cho and H. M. Kim, *Chem. Commun.*, 2012, **48**, 3518–3520.
45 K. Xu, L. He, X. Yang, Y. Yang and W. Lin, *Analyst*, 2018, **43**, 3555–3559.